MOX-Report No. 24/2017

Computational fluid-dynamic comparison between patch-based and direct suture closure techniques after carotid endarterectomy

Domanin, M.; Bissacco, D.; Le Van, D.; Vergara, C.

MOX, Dipartimento di Matematica
Politecnico di Milano, Via Bonardi 9 - 20133 Milano (Italy)

mox-dmat@polimi.it http://mox.polimi.it

COMPUTATIONAL FLUID-DYNAMIC COMPARISON BETWEEN PATCH-BASED AND DIRECT SUTURE CLOSURE TECHNIQUES AFTER CAROTID ENDARTERECTOMY

Maurizio Domanin MD [ab]
Daniele Bissacco MD [a]
Davide Le Van Eng [c]
Christian Vergara Prof [c]

a Department of Clinical Sciences and Community Health, Università di Milano, Italy
b Unità Operativa di Chirurgia Vascolare, Fondazione I.R.C.C.S. Cà Granda Ospedale Maggiore Policlinico, Milano, Italy,
c MOX, Dipartimento di Matematica, Politecnico di Milano, Italy.

Corresponding author:
Maurizio Domanin
Department of Clinical Sciences and Community Health, Università di Milano, Italy
Unità Operativa di Chirurgia Vascolare, Fondazione I.R.C.C.S. Ca' Granda Ospedale Maggiore Policlinico, Milano, Italy,
Via Francesco Sforza 35
20122 Milano, Italy.
Tel +39-2-55032438 Email: maurizio.domanin@unimi.it

Short title: CFD COMPARISON OF CLOSURE TECHNIQUE AFTER CEA

Disclosure
The authors have no personal, financial, or institutional interest in any of the drugs, materials, or devices described in this article.

ABSTRACT

Objective: To describe and analyze hemodynamic modifications in patients submitted to carotid endarterectomy (CEA) with different carotid closure techniques, using a computational fluid-dynamic (CFD) strategy, in order to identify disturbed flow conditions potentially involved in the development of restenosis.

Methods: Data from 8 carotid geometries in 7 asymptomatic patients who underwent CEA were analyzed. In six cases (A-F), CEA was performed using patch graft (PG) closure, while in two cases (G and H) direct suture (DS) closure was performed. Three-dimensional carotid geometries, derived from postoperative Magnetic Resonance Angiography, were reconstructed using a level-set segmentation technique. Where PG was originally used it was virtually removed, creating a virtual DS scenario (PG *vs* virtual-DS) while, on the contrary, in cases submitted to DS closure, a virtual PG was inserted (DS vs virtual-PG). Modified geometries were designed using visualization-dedicated software. CFD analysis was performed using the finite elements library LifeV and velocity data obtained from Doppler Ultrasound waveforms.

To compare hemodynamic effects, wall shear stress-based quantities were considered indicators of disturbed flow and thus favorable conditions for the development of restenosis. In particular, oscillatory shear index (OSI) and relative residence time (RRT) were calculated both for original and virtual scenarios.

Results: For the six original PG cases, we measured the following: Mean of averaged-in-space OSI of 0.07 ± 0.01 for PG and 0.03 ± 0.02 for virtual-DS (difference 0.04 ± 0.01; P=.0016). Mean of the percentage of area with OSI > 0.2 (%A-OSI > 0.2) 10.08% ± 3.38% (PG) and 3.80% ±

3.22% (virtual-DS) (difference 6.28 ± 1.91; P= .008). Mean of the averaged-in-space RRT 5.48 ± 3.40 1/Pa (PG) and 2.62 ± 1.12 1/Pa (virtual-DS) (difference 2.87 ± 1.46; P =.097). Mean %A RRT > 4 1/Pa of 26.53% ± 12.98% (PG) and 9.95% ± 6.53% (virtual-DS) (difference 16.58 ± 5.93; P= .025).

For the two original DS cases we measured the following: Averaged-in-space OSI 0.02 and 0.04 (DS) and 0.03 and 0.02 (virtual-PG), %A-OSI > 0.2, 0.9% and 7.6% (DS) and 3.0% and 2.2% (virtual-PG), averaged-in-space RRT 1.8 and 2.0 1/Pa (DS) and 2.9 and 1.9 1/Pa (virtual-PG), %A-RRT > 4.0 1/Pa: 6.8% and 9.8% (DS) 9.4% and 6.2% (virtual-PG). These results revealed generally higher disturbed flows in the PG configurations with respect to the DS ones.

Conclusions: OSI and RRT values were higher in PG cases with respect to virtual-DS ones, while, in direct contrast, the virtual insertion of PG gave conflicting results that were primarily determined by the original carotid geometries.

Keywords:

Cerebrovascular, Carotid pathophysiology, endarterectomy, recurrent stenosis, computational fluid dynamics, Wall shear stress

INTRODUCTION

The carotid bifurcation has a complex geometry that influences the local hemodynamics and consequently the development of atherosclerotic risk. [1-3] A similar situation occurs after carotid endarterectomy (CEA), where the geometric structure derived from the closure technique deeply influences hemodynamics, possibly leading to restenosis due to hyperplasia. [4]

Flow patterns with low and oscillating wall shear stresses (WSS) can promote both atheromatous plaque formation [5-7] and myointimal hyperplasia, the leading causes of restenosis development. [8-11] The choice of closure technique is an important issue in this process. Patch graft (PG) can be incorporated either routinely or selectively as in case of small diameter carotids). In any case, the question still arises as to whether it is better to employ PG or direct suture (DS).

Today, computational fluid dynamics (CFD) allows, thanks to tremendous advances in both mathematical models and computational resources, to perform qualitative and quantitative predictions of fluid flows, based, e.g., on the Finite Element Method. An interesting challenge for CFD studies is the carotid bifurcation, because WSS, which is not measurable by radiological or ultrasound technologies, might be accurately analyzed and calculated. [12]

The aim of this study was to provide a comparative CFD analysis between the two closure techniques performed in real carotid geometries. We have virtually designed DS closure in patients where PG was originally inserted. This allowed us to compare some WSS-based indices and to assess the effect of the closure technique on hemodynamics. Moreover, we considered the opposite scenario, in which PG closure was virtually drawn in two cases where DS had originally been

performed.

METHODS

Ethics Statement

The study has been approved by the I.R.C.C.S. Fondazione Policlinico Ethics Committee according to institutional ethics guidelines. All the patients gave their signed consent for the publication of data.

Clinical data

We have studied 8 carotid geometries (cases A to H in what follows) in 7 asymptomatic patients (6 females and 1 male), who underwent to CEA for carotid stenosis greater than 70%.

In all cases CEA was performed using a standard surgical technique that included longitudinal arteriotomy, 2.5x optical magnification and systemic heparin under regional block anesthesia.

Cases A and B were submitted to obligatory PG according to Guidelines [13-14], while in cases C-F, PG was used because of the presence of an ICA smaller than 5 mm. As a control, we analyzed two additional cases (G and H) submitted to DS because of the presence of an ICA diameter greater than 5 mm. In all cases, the carotid plaque was localized in the carotid bulb, but in one case (A) the plaque spread also to the CCA, while in 4 cases (B-D and F) the plaque spread to the ICA (Table I).

The PG insertion in cases A-F was performed using a 6 x 75 mm polyester collagen-coated patch (Ultra-thin Intervascular®, Mahwah, U.S.A) properly tailored and distally trimmed (last 3 mm) of

33% to give it a smoothly tapered transition. Sutures were all performed with a 6-0 non-absorbant monofilament polypropylene standard running suture line (Everpoint-M, Ethicon, Sommerville, U.S.A.). The closure of the arteriotomy for both PG and DS was measured in length and photographed, to record its localization and longitudinal positioning (Fig. 1a). No perioperative complications were observed and no shunts were necessary.

By means of a sterile caliper in the operative field, the average thickness of the suture line was determined to be equal to 1 mm in the PG cases. When DS was performed, the resulting suture line was more precise in order to spare the arterial wall; accordingly, we have measured an average bite of 0.8 mm.

Acquisition of Doppler Ultrasound signals

After CEA, all the bifurcations were sampled with Carotid Doppler Ultrasound **(**DUS) using an iU22 ultrasound scanner and linear 8 MHz probe (Philips Ultrasound, Bothwell, U.S.A). Velocities were measured 2 cm retrograde from the bifurcation in the common carotid artery (CCA), and 2 cm downstream from the bifurcation in the ICA with a beam-to-flow angle less than or equal to 60° at the center of the vessel, to record measures along the longitudinal axis.

Acquisition of radiological images and generation of the modified scenarios.

Three-dimensional carotid geometries, derived from postoperative Magnetic Resonance Angiography (MRA), performed with a 1.5 T Avanto MR scanner (Siemens, Munich, Germany) one month after CEA, were reconstructed using a level-set segmentation technique (VMTK http://www.vmtk.org) in order to obtain surface models of the boundary lumen (Fig. 1b-c).

A possible corresponding DS configuration was virtually designed for PG cases (A-F), as if the

patch had not been inserted during CEA. We refer in what follows to PG and virtual-DS to indicate the PG and DS configurations of cases A-F, respectively. To convert the closure configurations scenarios, we used the software Paraview (http://www.paraview.org).

In particular, on the boundary lumen surface we have virtually done the following:

- pinpointed the PG previously inserted at the carotid bifurcation after CEA;
- removed the PG, subtracting 6 mm from the carotid circumference and 4 mm from its distal end (last 3 mm) as result of its 30% trimming (Fig. 2a-c);
- added 1.0 mm for each side, i.e. 2.0 mm, as the effect of the removal of the PG's double suture line from the carotid wall;
- subtracted 0.8 mm, i.e., the loss of carotid wall tissue to perform the DS line.

To provide preliminary results about the potential validity of the arguments highlighted in this work, the opposite scenario was also considered: starting from the geometries of two patients where DS was originally performed, PG was virtually inserted (*DS* versus *virtual-PG*). In these cases, the original configurations have been provided by the DS ones, and the modified scenarios by the PG ones. To obtain conversion from DS to PG, we have done the following:

- pinpointed the DS previously performed at the carotid bifurcation after CEA;
- added 6.0 mm (i.e the width of the PG) to the carotid circumference and 4.0 mm (as result of 30% PG trimming) to its distal end (last 3 mm);
- subtracted 2.0 mm, i.e. the space needed to insert the PG for the double suture line on the arterial wall (1.0 mm for each side);
- added 0.8 mm, i.e. the space needed on the arterial wall for the bites of the single suture line

in DS.

For all the geometries considered (original and virtual), a tetrahedral volumetric mesh was generated for each patient (Fig. 1d and Fig. 2d). Mesh dimensions of original and modified geometries are reported in Table 2.

Numerical simulations and fluid-dynamic indices.

Blood dynamics were modeled by assuming blood as an incompressible homogeneous Newtonian fluid, under laminar and rigid wall assumptions. A CFD analysis was performed by using the finite elements library LifeV (http://www.lifev.org). Velocity data obtained from DUS signals have been used to prescribe patient-specific boundary conditions at the inlet (CCA) and outlet (ICA) both in the original and in the modified scenarios. In particular, flow rates have been estimated by means of the formula proposed by Ponzini et al. [15] and consequently prescribed by means of the Lagrange multiplier method. [16-17] At the ECA, we imposed a zero stress condition. We performed a refinement study with respect to time and space discretization parameters, by testing that the results on WSS remained the same, up to a tolerance of 2%, when separately and independently reducing the time and space steps.

Hemodynamic indices

The computed blood velocity was then elaborated to compute the WSS at the lumen boundary and the related indices used to assess the risk of restenosis, i.e., the oscillatory shear index (OSI) and relative residence time (RRT). These quantities are good indicators of low and oscillating WSS,

which is known to possibly lead to myointimal hyperplasia. [8, 10-11] In particular, we have computed the averaged-in-space OSI and RRT. To better emphasize the hemodynamic behaviour, we have also computed the percentage area (%A) of the lumen boundary surface with OSI values above 0.2 and with RRT above 4.0 1/Pa, thresholds that have been identified as reliable values to discriminate between disturbed and non-disturbed flow. [18-19]

Statistical analysis was then performed using JMP 11.2.0 (SAS Institute Inc, NC, USA). Student's T-test was used to determine statistically significant differences between two independent means of sampled data.

RESULTS

Analysis of Oscillatory Shear Index

Fig. 3 reports the spatial distribution of OSI for each patient in both the original and virtual scenarios. These results visually highlight the change in OSI distribution at the carotid bifurcation after the virtual intervention.

To better emphasize this behaviour, we show the averaged in space OSI and percentage of surface area (%A) with OSI > 0.2 for all the configurations (Table III). The averaged-in-space OSI was computed over the six cases (A-F) where PG were virtually removed, converting the intervention to the virtual-DS option. Then, a comparison between PG and virtual-DS results was performed. An average in space OSI of 0.07 ± 0.01 for PG *versus* 0.03 ± 0.02 for virtual-DS (difference 0.04 ± 0.01; P =.0016) was obtained. The same analysis for the %A-OSI > 0.2 was performed, obtaining

10.08 ± 3.38 % for PG *versus* 3.80 ± 3.22 % for virtual-DS (difference 6.28 ± 1.91; P =.008) (Table III).

In the opposite scenario, i.e., for the two DS cases (G and H) where the PG was virtually inserted (DS versus virtual-PG), the averaged-in-space OSI values were 0.02 and 0.04 for DS *versus* 0.03 and 0.02 for virtual-PG, respectively, while for %A-OSI > 0.2, 0.9 % and 7.6 % for DS *versus* 3.0 % and 2.2 % for virtual-PG were obtained.

Analysis of Relative Residence Time

Fig. 4 shows the RRT for each patient both in the original and in the virtual configurations. Also in this case, the results demonstrate a substantial reduction of the values related to WSS after the virtual removal of PG. To better emphasize this phenomenon, in Table IV we show the averaged-in-space RRT and %A-RRT > 4.0 1/Pa, for all the configurations considered.

In the six cases (A-F), where PG was virtually removed (PG versus virtual-DS), the averaged in space RRT was determined to be 5.48 ± 3.40 1/Pa for PG and 2.62 ± 1.12 1/Pa for virtual-DS (difference 2.87 ± 1.46; P = .097). The %A-RRT > 4 1/Pa resulted 26.53 ± 12.98 % for PG and 9.95 ± 6.53 % for virtual-DS (difference 16.58 ± 5.93; P = .025) (Table III).

In the opposite scenarios (G-H) where DS was virtually transformed in PG, the averaged-in-space RRT values were 1.8 and 2.0 1/Pa for DS and 2.9 and 1.9 1/Pa for virtual-PG, respectively, while %A-RRT > 4.0 1/Pa resulted 6.8% and 9.8% for DS *versus* 9.4% and 6.2 % for virtual-PG.

DISCUSSION

Background

Carotid endarterectomy is an effective surgical procedure used to reduce the risk of stroke in the case of an atherosclerotic plaque narrowing the carotid artery, but the optimal closure technique remains controversial. Since its introduction, PG was proposed to reduce recurrences rates [20-21] both in the early postoperative period, to avoid technical defects that could narrow the lumen caused by DS, and in the late postoperative period, when PG should minimize the hemodynamic effects of restenosis. PG should never be used to enlarge the site of CEA but rather to recreate the original shape of carotid bifurcation. [20]

PG incorporation needs a double suture line that increases carotid clamping time with an augmented risk of cerebral ischemia and patient discomfort in case of loco-regional anesthesia. [22] Moreover, the insertion of alloplastic material raises blood losses and the risk of severe complications such as infections or pseudo-aneurysms. [23-24] Indeed, the longer time required for carotid cross-clamping could increase the occurrence of neurocognitive deficits. [25]

Actually, the standard use of PG has been endorsed by the guidelines of the most relevant scientific society of vascular surgery, [13-14] as well as in several textbooks of vascular surgery, supported by the evidence of reduced 30-day and long term risk of stroke, deaths and lower rates of return to surgery obtained by meta-analysis of the outcomes of randomized clinical trials. [26] However, while a subsequent update which included more recent studies still supported the routine use of PG, it highlighted less robust results maintaining “just a borderline significant benefit" for PG. [27] Moreover, many further recent studies reported no higher complication rates or worse clinical

outcomes when PG was preferred. [28-31] Despite those recommendations, survey of vascular surgeons reported that individual preferences on this issue still vary widely. [32]

Hemodynamics is a well known determining factor in the growth of carotid atheromatous disease. Regions affected by low and oscillating WSS are associated with monocyte activation, increased vasoconstriction, oxidative stress, higher cellular turnover and apoptosis. [33] All these biological responses are mediated by endothelial cells with the elicitation of inflammatory processes that possibly lead to myointimal hyperplasia. Induction of myointimal hyperplasia is due to mechanical injury to the arterial wall and contributes to the growth of restenosis. [34]

OSI and RRT are robust WSS-derived indices of disturbed flow, widely used to investigate the role of hemodynamics at the carotid bifurcation in the development of atheromatous plaque and restenosis. [2, 35]

Archie et al., in their pioneering studies about the geometric changes of bifurcation after CEA, reported that PG has two major effects on carotid bifurcation geometry: an increase of bulb length and a more gradual transition of diameter toward the ICA. These geometrical modifications allow for a transitional reduction of diameter from the terminal common carotid bulb to the more distal internal carotid artery, while DS shows irrelevant effects with respect to preoperative geometry. [4]

The first mathematical models regarding the conditions of carotid arteries after CEA were proposed by Hyun et al. [9] This work focused on the analysis of WSS, particle deposition measures and their related long-term atherosclerotic restenosis potential.

Harloff et al., studying carotid bifurcations of healthy patients matched with patients submitted to eversion CEA using 4D MRA data, found that WSS is influenced by the individual carotid

geometries and that eversion CEA of previously high-grade ICA stenosis tends to recover WSS distributions similar to the physiological values observed in normal carotids. [36]

Kamenskiy et al., using CFD analysis in patients submitted to conventional CEA versus eversion CEA, observed that PG, by increasing bulb cross-sectional area and length, modifies carotid geometries. They reported wider areas of high OSI as a consequence of the abrupt diameter transition from PG to the distal native artery. [37]

Harrison et al., comparing in-vitro carotid bifurcation models of healthy bifurcations with DS and two different PG sizes (5 and 8 mm), observed that DS hemodynamic forces produced flow patterns similar to the healthy subjects and, when PG was used, that the tighter one offered a better hemodynamic behavior. [38]

In our previous studies, we have analysed by means of CFD the fluid–dynamics in carotid bifurcations after CEA. Both OSI and RRT values were higher when PG was preferred to DS and also the resulting areas with disturbed flow were wider. The highest absolute computed values were observed after indiscriminate PG closure regardless of carotid diameters. DS did not create negative hemodynamic conditions with potential adverse effects on long-term outcomes. [39-40] However, in those studies we did not perform the virtual modification proposed in this work, so that we could not compare PG and DS in the same geometries.

Computational studies of carotids have been performed on healthy and diseased vessels for two decades. In more recent times, many authors have stressed the importance of the use of patient-specific data in order to obtain reliable numerical results. [12, 39, 41-42] In particular, the use of real geometries and velocity data prescribed at the inlet and outlet remains a critical issue in order to

obtain reliable results in numerical simulations. However, for the cases considered in this work, we could obtain patient-specific clinical data to be used in the numerical simulations only in one of the two scenarios considered (PG or DS), depending on the real closure technique considered for the patient. The original contribution of this work was to virtually design the alternative closure technique for each patient, obtaining an otherwise impossible comparative CFD study of the two closure techniques.

Analysis of the results

Referring to Table I, for all the cases reported, it is important to note that CEA was always performed in the bulb region and so, when PG was inserted to close the arteriotomy, it resulted in enlargement an already wider anatomical location.

In our analysis, in all cases in which the PG was virtually removed and converted to the DS option, a statistically significant decrease in both OSI and %OSI > 0.2 was observed (Table III).

Colorimetric maps of the OSI values clearly display a consistent reduction after PG virtual removal as well as focal peaks that can be observed in cases A, C and E, next to the lower side of the suture line toward the CCA region (Fig. 3).

The RRT values computed after virtual DS closure decreased, compared to the values obtained with the original PG closure, although the differences did not reach the level of statistical significance as described in the Results section. Only in one case (E), where PG was originally inserted at the bulb level, we have observed a slight reduction of RRT values after virtual DS closure (respectively 2.3 1/Pa *versus* 2.2 1/Pa) (Table IV). With regard to %RRT > 4.0 1/Pa, in all

cases studied, the values measured for PG were significantly higher with respect to the values computed for virtual-DS (Table IV).

Comparing the colorimetric maps of RRT for virtual-DS with those obtained for the original PG, we observed in most cases a clear reduction in the magnitude of RRT and in the area with disturbed flow (A-D and F). A less significant result, with a different spatial distribution, was observed only in case E, probably due to the site where CEA was originally performed (Fig. 4). In particular, the focal point of the higher values of RRT were toward the CCA, but virtual-DS closure changed their localization to more pronounced peaks along the midline.

In the opposite scenario, after the virtual addition of the PG, we observed different hemodynamic behaviors. While in the first case (G), a rise of WSS-related indices passing from the DS to virtual-PG were discernable, in the second case (H) these values were unexpectedly reduced (Tables III and IV).

Furthermore, colorimetric maps confirmed this observation, showing in G a wider area of disturbed flow values, while in H a slight reduction of this phenomenon was observed (Fig. 3 and 4).

Even after the real DS closure, case H in fact showed for both OSI and RRT a particular "double shot" distribution at the opposite poles of the suture line, without evident involvement of the bulb region. Thus, in this particular case the virtual insertion of PG did not change local hemodynamics, but rather it further enhanced the focalization of disturbed flow in these two opposite areas.

From the hemodynamic point of view, the analysis of the virtually modified geometries generally seems to support the benefits of the selective use of PG, avoiding its use when CEA is performed only at the CCA or bulb level, or when ICA diameter is greater than 5.0 mm. [43] In fact, PG removal

did not seem to create potentially negative hemodynamic effects on the carotid bifurcation, but rather it seemed to allow for a reduction of the disturbed flow. On the contrary, the insertion of PG in an already wider carotid bifurcation could enhance disordered flow development, potentially involved in restenosis.

In any case, PG still maintains its fundamental clinical role, mainly in selected cases, to overcome specific technical problems occurring during CEA or in the presence of smaller diameter carotid arteries and for lesions confined to the distal ICA.

A potential limitation of this study is the assumption of rigid walls in the computational experiments despite the fact that it is well accepted for non-stenotic carotids since this assumption has little influence on the value of WSS and should not affect the results of our comparisons. The results of our CFD analysis have been previously validated in 6 of the 8 cases presented here, as the values of velocity determined with CFD matched values of ICA peak systolic velocity measured by DUS, deviating by less than 10%. [39]

We also realize that the threshold value used in our evaluation was smaller than the values reported in the literature (6.0 1/Pa), however the qualitative conclusions were comparable. [19]

Other limitations of this study are related to the impossibility to perform direct validation of CFD results in the virtual geometries, and to the absence of assessment of the biological factors involved in the evolution of restenosis.

Conclusions

The purpose of this study was to investigate the effects of the virtual removal or addition of PG after CEA on carotid hemodynamics.

We have found that the obligatory use of PG, compared in the same carotid bifurcation to the virtual DS, seemed to create negative hemodynamic patterns possibly leading to development of myointimal hyperplasia or atherosclerosis. The formation of disturbed flow is strictly dependent on arterial geometries. Thus, an indiscriminate artificial enlargement due to the PG insertion in the carotid section could create pernicious flows which paradoxically could enhance restenosis instead of preventing it.

Predictive computational planning could drive the surgeon to improve the outcomes of CEA by reducing development of hemodynamic conditions favorable to recurrences.

Disclosures: None

Acknowledgments:

The authors acknowledge Edward Kiegle for his revision of English grammar.

REFERENCES

1. Thomas JB, Antiga L, Che SL, Milner JS, Steinman DA, Spence JD, et al. Variation in the carotid bifurcation geometry of young versus older adults: implications for geometric risk of

atherosclerosis. *Stroke.* 2005;36:2450-6.

2. Lee SW, Antiga L, Spence JD, Steinman DA. Geometry of the carotid bifurcation predicts its exposure to disturbed flow. *Stroke.* 2008;39:2341-7
3. Phan TG, Beare RJ, Jolley D, Das G, Ren M, Wong K et al. Carotid artery anatomy and geometry as risk factors for carotid atherosclerotic disease. *Stroke*. 2012;43:1596-1601.
4. Archie JP Jr. Geometric dimension changes with carotid endarterectomy reconstruction. *J Vasc Surg.* 1997;25:488-98.
5. Zarins CK, Giddens DP, Bharadvaj BK, Sottiurai VS, Mabon RF, Glagov S. Carotid bifurcation atherosclerosis. Quantitative correlation of plaque localization with flow velocity profiles and wall shear stress. *Circ Res.* 1983;53:502-14.
6. Ku DN, Giddens DP, Zarins CK, Glagov S. Pulsatile flow and atherosclerosis in the human carotid bifurcation. Positive correlation between plaque location and low oscillating shear stress. *Arteriosclerosis.* 1985;5:293-302.
7. Nixon AM, Gunel M, Sumpio BE. The critical role of hemodynamics in the development of cerebral vascular disease. *J Neurosurg.* 2010;112:1240-53.
8. Bassiouny HS, White S, Glagov S, Choi E, Giddens DP, Zarins CK. Anastomotic intimal hyperplasia: Mechanical injury or flow induced. *J Vasc Surg.* 1992;15:708–17.
9. Hyun S, Kleinstreuer C, Archie JP. Computer simulation and geometric design of endarterectomized carotid artery bifurcations. *Crit Rev Biomed Eng* 2000;28:53–9.
10. Meyerson SL, Skelly CL, Curi MA, Shakur UM, Vosicky JE, Glagov S et al. The effects of extremely low shear stress on cellular proliferation and neointimal thickening in the failing bypass graft. *J Vasc Surg* 2001;34:90-7.
11. Heisea M, Krügerb U, Rückertc R, Pfitzmana R, Neuhausa P, Settmachera U. Correlation of intimal hyperplasia development and shear stress sistribution at the distal end-side-anastomosis, in vitro study using particle image velocimetry. *Eur J Vasc Endovasc Surg*. 2003;26:357–66.
12. Groen HC, Simons L, Van Den Bouwhuijsen QJ, Bosboom EM, Gijsen FJ, van der Giessen

AG, van de Vosse FN et al. MRI-based quantification of outflow boundary conditions for computational fluid dynamics of stenosed human carotid arteries. *J Biomech.* 2010;43:2332-38.

13. Brott TG, Halperin JL, Abbara S, Bacharach JM, Barr JD, Bush RL et al. 2011 ASA/ACCF/AHA/AANN/AANS/ACR/ASNR/CNS/SAIP/SCAI/SIR/SNIS/SVM/SVS guideline on the management of patients with extracranial carotid and vertebral artery disease. *Circulation*. 2011;124:e54-130.
14. Liapis CD, Bell PR, Mikhailidis D, Sivenius J, Nicolaides A, Fernandes e Fernandes J et al. ESVS guidelines. Invasive treatment for carotid stenosis: indications, techniques. *Eur J Vasc Endovasc Surg.* 2009;37:1-19.
15. Ponzini R, Vergara C, Redaelli A, Veneziani A. Reliable CFD-based estimation of flow rate in haemodynamics measures. *Ultrasound in Medicine and Biology.* 2006;32:1545-55.
16. Formaggia L, Gerbeau JF, Nobile F, Quarteroni A. Numerical treatment of defective boundary conditions for the Navier-Stokes equation. *SIAM J Num Anal.* 2002;40:376-401.
17. Veneziani A, Vergara C. Flow rate defective Boundary Conditions in Haemodynamics Simulations. *International Journal for Numerical Methods in Fluids.* 2005;47:803-16.
18. Morbiducci U, Ponzini R, Rizzo G et al. Mechanistic insight into the physiological relevance of helical blood flow in the human aorta: an in vivo study. *Biomech Model Mechanobiol.* 2011;10:339–55.
19. Gallo D, De Santis G, Negri F et al. On the use of in vivo measured flow rates as boundary conditions for image-based hemodynamic models of the human aorta: implications for indicators of abnormal flow. *Ann Biomed Eng.* 2012;40:729–41.
20. Imparato AM. The role of patch angioplasty after carotid endarterectomy. *J Vasc Surg.* 1988;7:715-6.
21. Deriu GP, Ballotta E, Facco E et al. Stroke risk reduction in asymptomatic and symptomatic patients treated surgically: the effectiveness of carotid endarterectomy with patch graft angioplasty. *Eur J Vasc Surg.* 1988;2:87-91.

22. Stoneham MD, Knighton JD Regional anaesthesia for carotid endarterectomy, *Br J Anaesth*, 1999;82:910–9.
23. Naylor AR, Payne D, London NJM, Thompson MM, Dennis MS, Sayers RD et al. Prosthetic patch infection after carotid endarterectomy. *Eur J Vasc Surg.* 2002;23:11-6.
24. Branch CL Jr, Davis CH Jr. False aneurysm complicating carotid endarterectomy. *Neurosurgery.* 1986;19:421-5.
25. Meyer EJ, DeLaPaz R, Halazun HJ, Rampersad A, Sciacca R, Zurica J et al. Neuropsychological dysfunction in the absence of structural evidence for cerebral ischemia after uncomplicated carotid endarterectomy. *Neurosurgery.* 2006;58:474-80.
26. Bond R, Rerkasem K, AbuRahma AF, Naylor AR, Rothwell PM. Patch angioplasty versus primary closure for carotid endarterectomy. *Cochrane Database Syst Rev.* 2004:CD000160.
27. Rerkasem K, Rothwell PM. Systematic review of randomized controlled trials of patch angioplasty versus primary closure and different types of patch materials during carotid endarterectomy. *Asian J Surg.* 2011;34:32-40.
28. Zenonos G, Lin N, Kim A, Kim JE, Governale L, Friedlander RM. Carotid endarterectomy with primary closure: analysis of outcomes and review of literatures. *Neurosurgery.* 2012;70:646-55.
29. Malas M, Glebova NO, Hughes SE, Voeks JH, Qazi U, Moore WS et al. Effect of patching on reducing restenosis in the carotid revascularization endarterectomy versus stenting trial. *Stroke.* 2015;46:757-61.
30. Maertens V, Maertens H, Kint M, Coucke C, Blomme Y. Complication rate after carotid endarterectomy comparing patch angioplasty and primary closure. *Ann Vasc Surg*. 2016;30:248–52.
31. Avgerinos ED, Chaer RA, Naddaf A, El-Shazly OM, Marone L, Makaroun MS. Primary closure after carotid endarterectomy is not inferior to other closure techniques. *J Vasc Surg.* 2016;64:678-83.
32. Harrison G, Brennan J, Naik J, Vallabhaneni S, Fisher R. Patch variability following carotid

endarterectomy: a survey of Great Britain and Ireland. *Ann R Coll Surg Engl* 2012;94:411-5.

33. Malek AM, Alper SL, Izumo S. Hemodynamics shear stress and its role in atherosclerosis. *JAMA.* 1999;282:2035-42.
34. Mattsson EJ1, Kohler TR, Vergel SM, Clowes AW. Increased blood flow induces regression of intimal hyperplasia. *Arterioscler Thromb Vasc Biol.* 1997;17:2245-9.
35. Ding Z, Wang K, Li J, Cong X. Flow field and oscillatory shear stress in a tuning-fork-shaped model of the average human carotid bifurcation. *J Biomech* 2001;34:1555-62.
36. Harloff A, Berg S, Barker AJ, Schöllhorn J, Schumacher M, Weiller C et al. Wall shear stress distribution at the carotid bifurcation: influence of eversion carotid endarterectomy. *Eur Radiol.* 2013;23:3361–9.
37. Kamenskiy AV, Pipinos II, Dzenis YA, Gupta PK, Jaffar Kazmi SA, MacTaggart JN. A mathematical evaluation of hemodynamic parameters following carotid eversion and conventional patch angioplasty. *Am J Physiol Heart Circ Physiol.* 2013;305:H716-4.
38. Harrison GJ, How TV, Poole RJ, Brennan JA, Naik JB, Vallabhaneni SR et al. Closure technique after carotid endarterectomy influences local hemodynamics, *J Vasc Surg.* 2014;60,418–27.
39. Guerciotti B, Vergara C, Azzimonti L, Forzenigo L, Biondetti P, Domanin M. Computational study of the fluid-dynamics in carotids before and after endarterectomy. *Journal of Biomechanics.* 2016;49:26-38.
40. Domanin M, Buora A, Scardulla F, Guerciotti B, Forzenigo L, Biondetti P et al. Computational fluid-dynamic analysis after carotid endarterectomy: patch graft versus direct suture closure . *Ann Vasc Surg* 2017; (in press). 10.1016/j.avsg.2017.04.016
41. Campbell IC, Ries J, Dhawan SS, Quyyumi AA, Taylor WR, Oshinski JN. Effect of inlet velocity profiles on patient-specific computational fluid dynamics simulations of the carotid bifurcation. *J Biomech Eng.* 2012;134:051001.
42. Wake AK, Oshinski JN, Tannenbaum AR, Giddens DP. Choice of in vivo versus idealized velocity boundary conditions influences physiologically relevant flow patterns in a subject-

specific simulation of flow in the human carotid bifurcation. *J Biomech Eng.* 2009;131:021013.

43. Golledge J, Cuming R, Davies AH, Greenhalgh RM. Outcome of selective patching following carotid endarterectomy. *Eur J Vasc Endovasc Surg*. 1996;11:458-63.

FIGURES LEGENDS

Fig.1

Exemplification of the workflow (case B). a) Identification of the localization of the PG during surgery; b) Segmentation of carotid bifurcation after CEA provided by VMTK; c) Surface models of the carotid bifurcation; d) Volumetric mesh of the patched carotid bifurcation

Fig. 2

Exemplification of the workflow (case B - continuation). a) Measurement of PG; b) Localization of the surface model; c) Virtual subtraction of the PG from the surface model; d) Creation of the new volumetric mesh after removal of PG.

Fig. 3

Colorimetric maps of OSI distribution on the lumen boundary computed in PG and corresponding virtual-DS (cases A-F), and in DS and corresponding virtual-PG (cases G-H).

Fig. 4

Colorimetric maps of RRT distribution on the lumen boundary computed in PG and corresponding virtual-DS (cases A-F), and in DS and corresponding virtual-PG (cases G-H).

Tab 1 – Classification of sex (F female; M male), localization of the carotid blockage (CCA Common carotid artery; B Bulb; ICA Internal carotid artery), side (R right; L left) and original intervention (PG Patch graft; DS Direct suture).

CASE	SEX	LOCALIZATION OF PLAQUE	SIDE	ORIGINAL INTERVENTION
A	F	CCA, B	R	PG
B	F	B	L	PG
C	F	B, ICA	R	PG
D	F	B, ICA	R	PG
E	F	B	L	PG
F	F	B, ICA	L	PG
G	F	B, ICA	R	DS
H	M	B	L	DS

Tab. 2 – Number of tetrahedra of the original and virtual computational meshes

CASE		ORIGINAL INTERVENTION		VIRTUAL INTERVENTION
		Number of tetrahedra (x 10^5)		Number of tetrahedra (x 10^5)
A	PG	1.3	DS	1.3
B	PG	1.0	DS	1.1
C	PG	1.8	DS	1.8
D	PG	2.0	DS	1.9
E	PG	2.4	DS	2.4
F	PG	6.6	DS	6.6
G	DS	3.5	PG	3.6
H	DS	2.4	PG	2.5

Tab. 3 Values of the averaged in space Oscillatory Shear Index (OSI) and percentage of area above the threshold in the original and virtual configurations

CASE		Original Intervention			Virtual Intervention	
		OSI	%A with OSI > 0.2 (%)		OSI	%A with OSI > 0.2 (%)
A	PG	0.09	11.6	DS	0.03	4.7
B	PG	0.09	15.7	DS	0.02	1.7
C	PG	0.07	10.4	DS	0.06	6.8
D	PG	0.06	9.0	DS	0.01	0.2
E	PG	0.07	7.8	DS	0.05	8.1
F	PG	0.06	6.0	DS	0.02	1.3
G	DS	0.02	0.9	PG	0.03	3.0
H	DS	0.04	7.6	PG	0.02	2.2

Tab. 4 – Values of the averaged in space Relative Residence Time (RRT) and percentage of area above the threshold in the original and virtual configurations

CASE		Original intervention			Virtual intervention	
		RRT (1/Pa)	%A RRT > 4.0 1/Pa (%)		RRT (1/Pa)	%A RRT > 4.0 1/Pa (%)
A	PG	5.7	34.6	DS	3.0	10.0
B	PG	11.3	43.6	DS	3.0	8.9
C	PG	7.2	35.8	DS	4.4	21.5
D	PG	3.6	16.2	DS	1.3	2.6
E	PG	2.2	13.0	DS	2.3	11.5
F	PG	2.9	16.0	DS	1.7	5.2
G	DS	1.8	6.8	PG	2.9	9.4
H	DS	2.0	9.8	PG	1.9	6.2

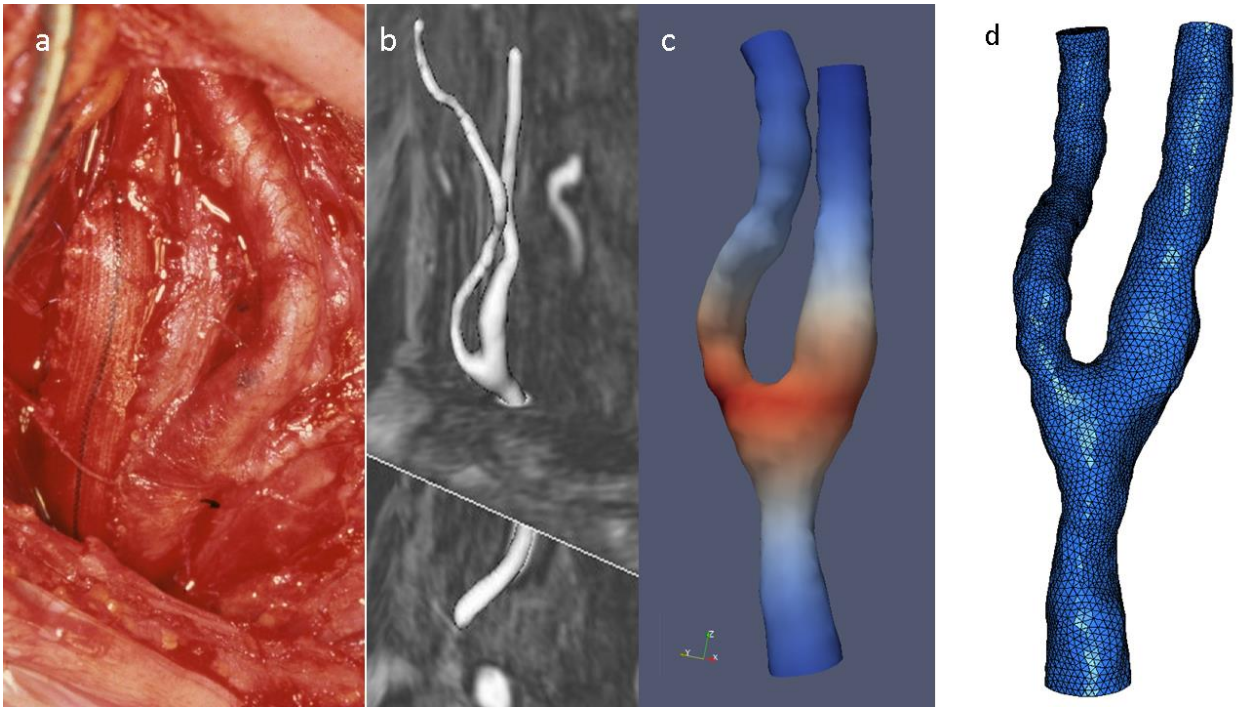

Figure 1

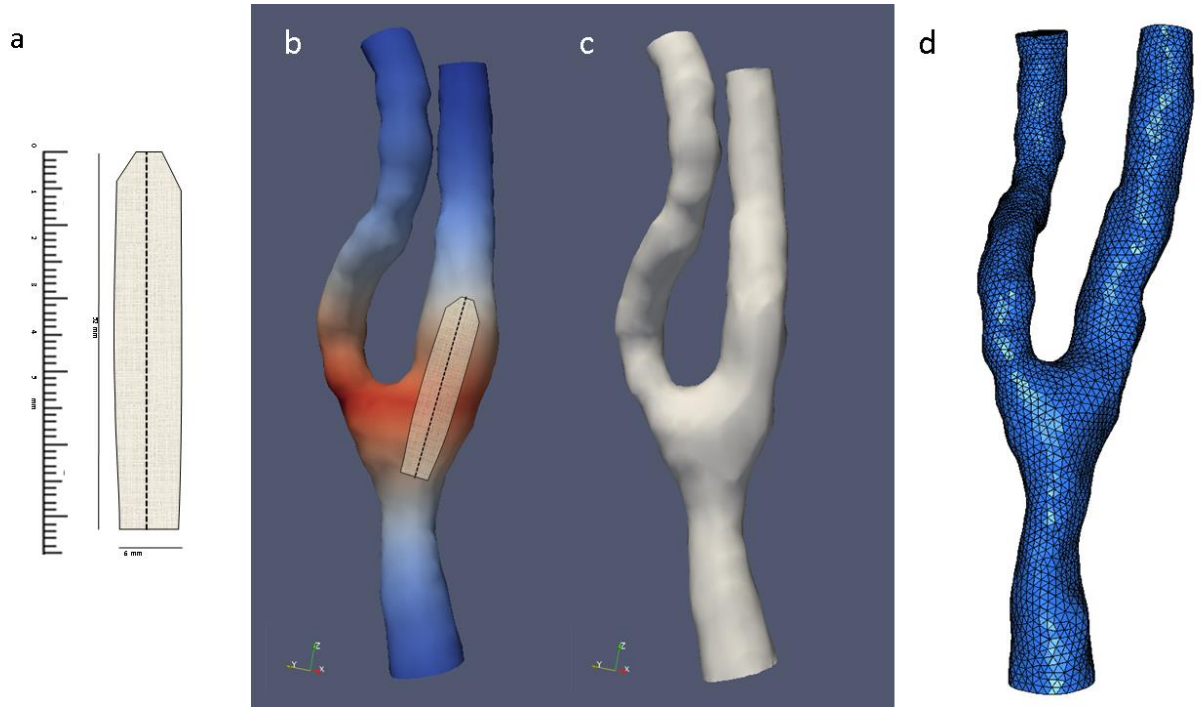

Figure 2

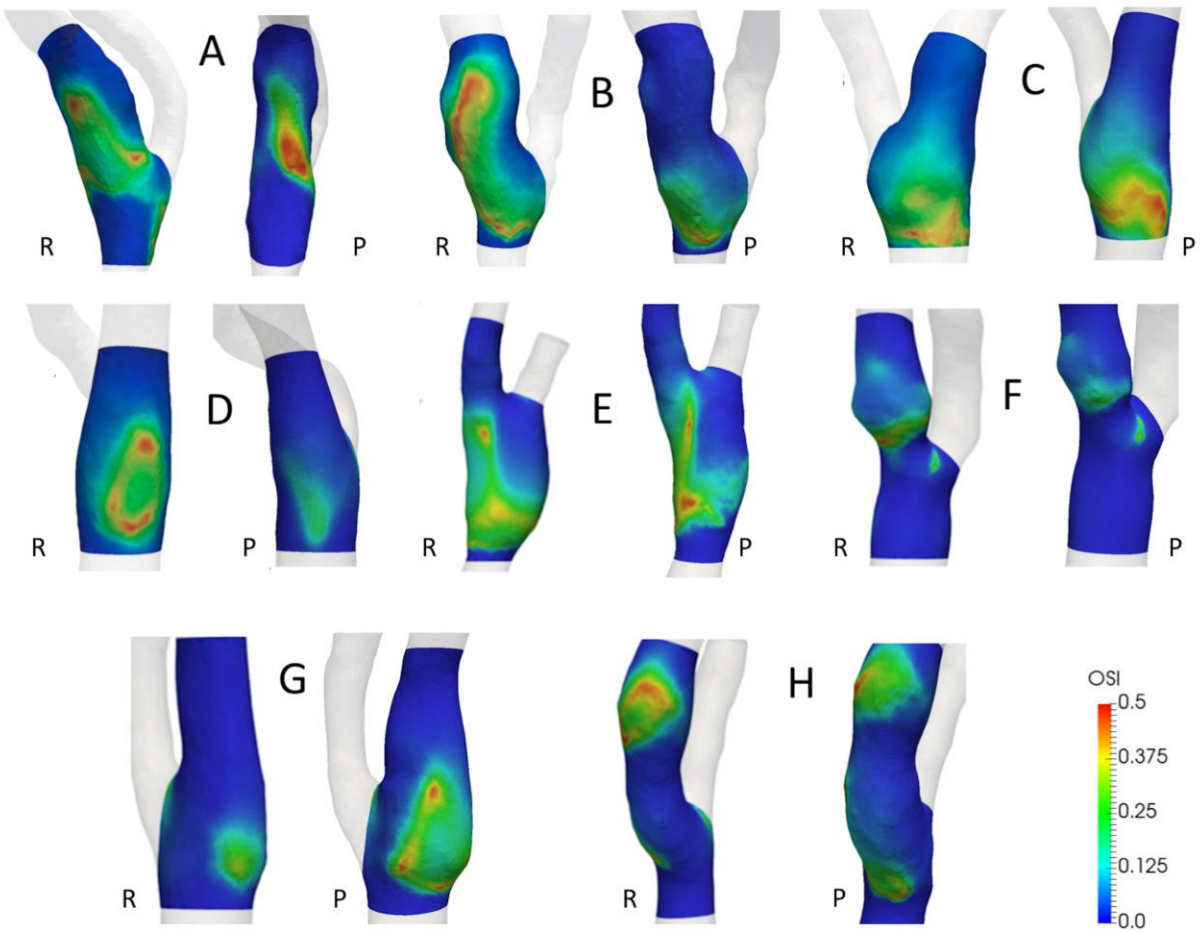

Figure 3

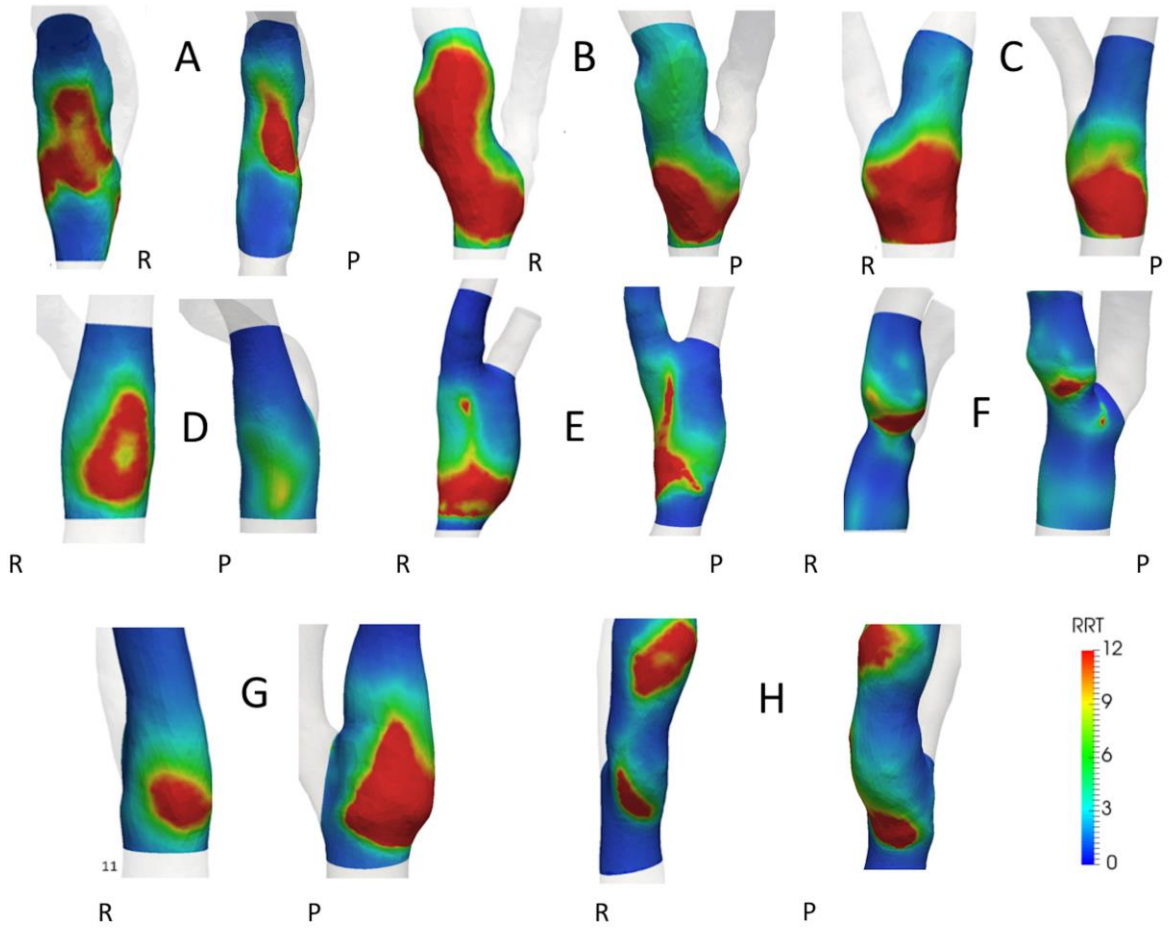

Figure 4

MOX Technical Reports, last issues

Dipartimento di Matematica
Politecnico di Milano, Via Bonardi 9 - 20133 Milano (Italy)

23/2017 Quarteroni, A.; Vergara, C.
Computational models for hemodynamics

21/2017 Talska, R.; Menafoglio, A.; Machalova, J.; Hron, K.; Fiserova, E.
Compositional regression with functional response

22/2017 Bartezzaghi, A.; Dede', L.; Quarteroni, A.
Biomembrane modeling with Isogeometric Analysis

18/2017 Ambartsumyan, I.; Khattatov, E.; Yotov, I.; Zunino, P.
A Lagrange multiplier method for a Stokes-Biot fluid-poroelastic structure interaction model

19/2017 Giovanardi, B.; Formaggia, L.; Scotti, A.; Zunino P.
Unfitted FEM for modelling the interaction of multiple fractures in a poroelastic medium

20/2017 Albrecht G.; Caliò F.; Miglio E.
Fair surface reconstruction through rational triangular cubic Bézier patches

14/2017 Bruggi, M.; Parolini, N.; Regazzoni, F.; Verani, M.
Finite Element approximation of an evolutionary Topology Optimization problem

16/2017 Ghiglietti, A.; Scarale, M.G.; Miceli, R.; Ieva, F.; Mariani, L.; Gavazzi, C.; Paganoni, A.M.; E
Urn models for response-adaptive randomized designs: a simulation study based on a non-adaptive randomized trial

15/2017 Tagliabue, A; Dede', L.; Quarteroni A.
Complex blood flow patterns in an idealized left ventricle: a numerical study

13/2017 Gigante, G.; Vergara, C.
Optimized Schwarz Methods for circular flat interfaces and geometric heterogeneous coupled problems